Action Potential Detection Algorithm Adaptable to Individual Nerve and Recording Setup

Romain Raffoul
BEAMS department
Université Libre de Bruxelles
Brussels, Belgium
romain.raffoul@ulb.be

Javier Chávez Cerda
BEAMS department
Université Libre de Bruxelles
Brussels, Belgium
javier.chavez.cerda@ulb.be

Elena Acedo Reina
Institute of Neuroscience
Université Catholique de Louvain
Brussels, Belgium
elena.acedoreina@uclouvain.be

Hugo Smets
BEAMS department
Université Libre de Bruxelles
Brussels, Belgium
hugo.smets@ulb.be

Maxime Verstraeten
BEAMS department
Université Libre de Bruxelles
Brussels, Belgium
maxime.verstraeten@ulb.be

Louis Vande Perre
BEAMS department
Université Libre de Bruxelles
Brussels, Belgium
louis.vande.perre@ulb.be

Rami Taheri
BEAMS department
Université Libre de Bruxelles
Brussels, Belgium
rami.taheri@ulb.be

Pascal Doguet
Synergia Medical SA
Mont -Saint-Guibert, Belgium
pascal.doguet@synergiam.com

Jean Delbeke
Institute of Neuroscience
Université Catholique de Louvain
Brussels, Belgium
jean.delbeke@uclouvain.be

Riëm El Tahry
Institute of Neuroscience
Université Catholique de Louvain
Brussels, Belgium
riem.eltahry@uclouvain.be

Jacques Deviere
LGE department
Université Libre de Bruxelles
Brussels, Belgium
jacques.deviere@ulb.be

Antoine Nonclercq
BEAMS department
Université Libre de Bruxelles
Brussels, Belgium
antoine.nonclercq@ulb.be

***Abstract*—This work presents an automated analysis algorithm to detect action potentials (APs) in a nerve and quantify its activity. The algorithm is based on template matching. The templates are automatically adapted to individual AP shapes that vary depending on the nerve fibers from which the AP originates, and the recording setup used. The algorithm was validated by quantifying vagus nerve activity recorded during in vivo experiments in a rat model. The MATLAB version of the code is available in open access on GitHub[1].**

Keywords—Action Potential detection, algorithm, vagus nerve, signal processing, template matching, clustering.

I. Introduction

The nervous system transmits information through action potentials (APs). AP recording can be challenging as the amplitude of neural signals recorded with cuff electrodes is typically 3 – 10 µV [1]. Although above the noise level of the electrode interface (< 0.5 μV_{RMS} [2]), this is much lower than the amplitude of many artifacts (e.g., muscular artifacts are up to typically 15 mV_{p-p} [1]). Besides, a typical recording can contain around 100 APs per second [3]. Manual counting is, therefore, nearly impossible for long-term recordings.

Algorithms are required to analyze the nerve activity, which is usually mainly performed by detecting the occurring APs and quantifying them in terms of frequency and amplitude. Besides, classifying them according to their shape could lead to discrimination among propagation speed and, therefore, discriminate the types of fibers that are activated [4].

AP detection algorithms have been widely reported in the literature. They can be roughly placed into three categories: simple amplitude thresholding [5], signal decomposition according to the frequency components [6], [7], and template matching [8], [9].

For single amplitude thresholding, the APs are expected to have an amplitude greater than the background level. AP can thus be distinguished using a minimum amplitude threshold. Harrison et al. proposed a circuit-integrated algorithm [5]. The main drawback of this technique is that the ground hypothesis is not always verified since the signal-to-noise ratio of recorded nervous signals varies greatly for each application (e.g. -30 dB reported for the human tibial nerve [10] and 1.2 to 3.8 dB in sciatic nerves of rats [11]). Besides, transient artifacts and interferences are often as large or larger than APs.

In the signal decomposition method, the signal is decomposed into different time-frequency components to separate the background and noise from the APs. Algorithms using an empirical mode decomposition of the signal, based on the band-limited frequential composition of APs, have been previously reported [6], [12]. The first four intrinsic mode functions of the empirical mode decomposition, containing the components of the APs, are kept. APs are detected when the amplitude of these layers is higher than a given threshold. This method assumes that the background/noise has a Gaussian distribution (verified in a first approximation [13]) and that the AP amplitude is higher than the background and noise. This method does not require prior knowledge of the shape of the APs, except for their main frequency components. It yields better results than a simple amplitude thresholding method [12]. However, artifacts

[1] https://github.com/BEAMS-Biomechatronics/AP-Detection-Algorithm

This work was supported by the Fonds de la Recherche Scientifique - FNRS under Grant(s) n° 40009012.

containing components in the same bandwidth as the APs cannot be filtered easily.

For template matching, a similarity measure is used to compare patterns in the signal with a template expected to represent the AP's shape [8], [9]. A thresholding is applied to this similarity measure to detect APs. However, the shape of the APs can vary widely depending on the activated nerve fibers and the recording setup that is used [4]. Hence, finding a proper template that suits all cases can be difficult.

We present here an algorithm based on template matching that can be used for processing other neural recordings, by applying automatic template adaptation to each individual AP shape. The method was validated in vivo with acute vagus nerve electroneurograms (VENG) recorded in a single rat.

The MATLAB R2021b (Mathworks, USA) version of the code is available in open access on GitHub[2].

II. Materials And Methods

The AP detection algorithm was inspired by an interictal spike detection algorithm used in electroencephalogram recordings [14], adapted here for detecting APs in nerve recordings. There are three main parameters, in the form of thresholds. We performed an in vivo trial to assess the quality of the output.

A. AP Detection Algorithm Workflow

The workflow of the algorithm is presented in Fig. 1.

The algorithm works in six steps. (1) The signal is filtered. (2) Templates of the targeted pattern are loaded. (3) APs are detected with the highest detection sensitivity settings. (4) Detected APs are separated into clusters according to their shape. The number of clusters is automatically adjusted to the number of major shapes. (5) Centroid shapes of the compounded clusters are used as templates for more specific AP detections, therefore adapting to the types of AP morphology. (6) Detected APs are summed and further validated based on their characteristics.

1) Signal filtering

First, the signal is digitally filtered in a tunable bandpass (second-order Butterworth back/forth zero dephasing). The default bandwidth is set to 300 Hz - 3,000 Hz.

2) Creation of the generic templates

The user defines the generic templates. By default, a single generic template has been used, presented in Fig. 2a. This template was based on a typical vagus nerve AP shape [4].

Alternatively, multiple templates can be chosen. In that case, the following steps of the algorithm are individually computed for each template and detected APs are regrouped.

3) Generic template matching detection

A first detection is performed by comparing the generic template with the nerve recording. The cross-correlation quantifies the similarity between the generic template and a sliding window of the signal. The examined frame and the template are normalized in amplitude, limiting the correlation value to the range [0, 1] (one corresponding to a perfect match). This allows focusing on the shape of the AP while removing the impact of the absolute amplitude, which largely

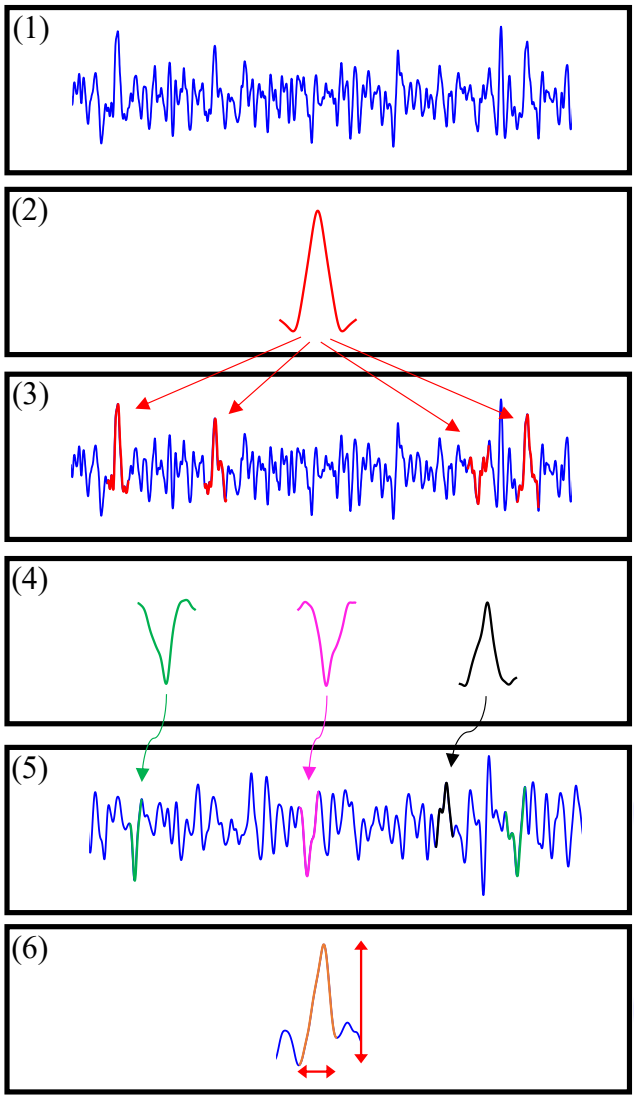

Fig. 1. Workflow of the algorithm: (1) Signal filtering; (2) Creation of the generic templates; (3) Generic template matching detection; (4) Clustering; (5) Subject-specific template matching detection; (6) Characteristic-based APs validation.

fluctuates depending on the recording setup. Potential APs are detected when the correlation is above a given threshold.

The amplitude of each potential AP is estimated by the difference between the maximum and minimum values in a 2 ms window around the top of the correlation. The amplitude of each potential APs is compared to the amplitude of the background signal, estimated by the local RMS amplitude on a 0.5 s window. Potential APs are discarded either if they are too large – considered as artifacts – or too small – considered as noise.

4) Clustering

The APs are clustered in the temporal domain using the K-means method. This clustering method aims to group the APs with the same shape, determining the patterns that repeatedly occur in the neural signal. The number of clusters is automatically determined to adapt to the number of AP shapes – and hence of activated fiber types – in the recording. In that regard, our method does not require prior knowledge on the number of different APs morphologies within the recording to determine the number of clusters needed for the

[2] https://github.com/BEAMS-Biomechatronics/AP-Detection-Algorithm

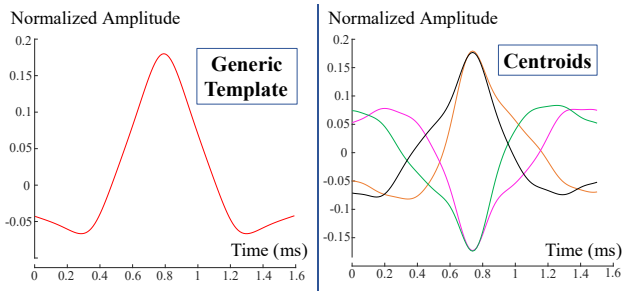

Fig. 2. Templates for the two detection. On the left, the generic template used for the first detection (step 3). On the right, the centroids for the clustering used as templates for the second detection (step 5).

detection. Starting from two clusters, the number of clusters increases until the APs in each cluster are believed to be too similar. This was estimated with a maximum mean discorrelation within each cluster lower than a given threshold. Clusters representing less than 1 % of the total APs processed are rejected as considered being non-repetitive enough to be physiological.

5) Nerve and recording setup specific template matching detection

A second AP detection is performed, similarly to the detection performed in step 3 with the centroid shapes obtained by the clustering method (step 4) used as the new APs templates.

6) Characteristic-based APs validation

Potential APs, detected during the previous step, are further validated based on their characteristics. The amplitude and duration of the AP are extracted for each potential AP. The APs that do not fit the amplitude are discarded.

B. Major Parameters

The three main thresholds are the two cross-correlations from the detections and the mean discorrelation level admitted within a cluster. More permissive parameters (i.e., lower cross-correlation thresholds and higher mean discorrelation authorized) will therefore allow the detection of a broader range of APs with different shapes but detects more false APs too.

Even if a two-step detection algorithm is used (step 3 and step 5) to adapt to each AP shape, the initial APs found are still influenced by the generic templates given as input during step 3. The extent to which the detected APs are related to the generic templates depends on the correlation thresholds used during the first and second detections (steps 3 and 5). In that regard, the algorithm is flexible and can be adapted to various applications. For instance, when choosing high correlation thresholds (i.e., focusing on APs that are similar to the generic template), one could either focus on the activity of specific fibers like in [4], work with different types of nerves, or adapt to different electrode spacings when recording in bipolar mode. Multiple templates can also be used to cover a range of activities at once without overlapping duplicates. A standard set of values for the in vivo validation is 0.8 and 0.85 for the first and second correlation threshold respectively, and 0.14 for the mean discorrelation.

C. In Vivo Validation

An acute VENG signal recorded on one rat was processed to validate the algorithm. There is unfortunately no “gold standard” in AP analysis. However, the vagus nerve is known to regulate the respiratory rhythm [15]. Therefore, the presence of a frequency and an amplitude modulation component following the respiratory rate was chosen as a criterion for assessing detected APs.

The measurements were performed on one male Wistar rat (2.5 months and 300 g). The rat was injected with Xylazine 7 mg/kg and Ketamine 100 mg/kg intraperitoneally (i.p.). A tripolar cuff electrode built following [16] was implanted on the cervical left vagus nerve. The two external electrodes are separated by 8 mm. In addition to the VENG, the electrocardiogram (ECG) was recorded from which the reference rate could be estimated. This experimental procedure has been approved by the University Health Sciences Sector Laboratory Animal Protection Committee (2018/UCL/MD/001). A detailed surgery description was previously reported in [17], [18].

The VENG hardware used for signal conditioning was a Sallen-Key bandpass filter 12-10000 Hz, Gain 900. For ECG, a Sallen-key bandpass filter 15-7000 Hz, Gain 900. The signals were digitized with a USB-6212 multifunction I/O device (National Instruments, Austin, USA) for an overall resolution of 0.17 µV/bit. The VENG was recorded with a sampling rate of 80 kHz and the ECG at 40 kHz, both for 3.5 minutes.

MATLAB R2021b (Mathworks, USA) was used to process the signal. The respiratory rate was derived from the ECG (referred to as ECGr) as developed in [19], [20]. The single initial template used, and the centroids of the clustering applied to the APs detected in step (3) are presented in Fig. 2b.

III. Results

The electrode loop impedance measured in a saline solution was 15 kΩ ± 5 kΩ, in line with our experience (10 kΩ - 20 kΩ). Our cuff electrode was subsequently implanted. The VENG consisted of high and lower amplitude bursts synchronous to respiration and heartbeat, respectively, as previously reported [17]. A sample of the signal is presented in Fig. 3. Bursts consisted of predominantly positive and negative APs with an amplitude of ~ 20 µVpp.

An illustration of the filtered VENG and detected APs are presented in Fig. 4. By computing the mean frequency and mean amplitude of the APs on a 0.15 s sliding window, we can analyze the modulation of the neural data.

The FFT spectrum of the ECGr, chosen as a reference physiological signal, shows a respiratory rhythm of 0.98 Hz (Fig. 5c). The APs detected by the algorithm show modulation in amplitude and frequency with main intrinsic frequency components at 0.986 Hz and 0.977 Hz, respectively (Fig. 5a-

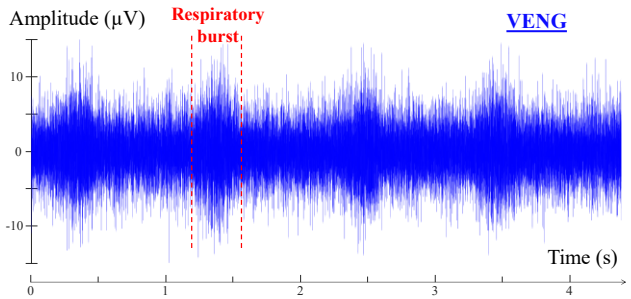

Fig. 3 Acute VENG signal. Respiratory-related bursts are visible.

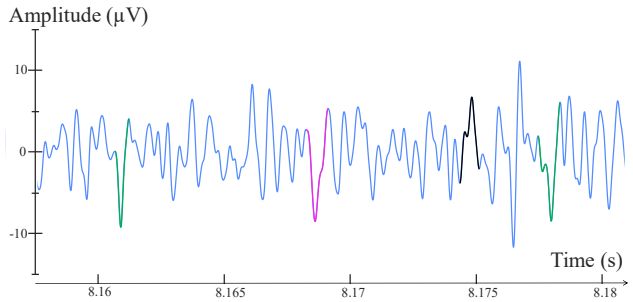

Fig. 4. Spikes detected with the algorithm. Each color of spikes comes from a different subject-specific template.

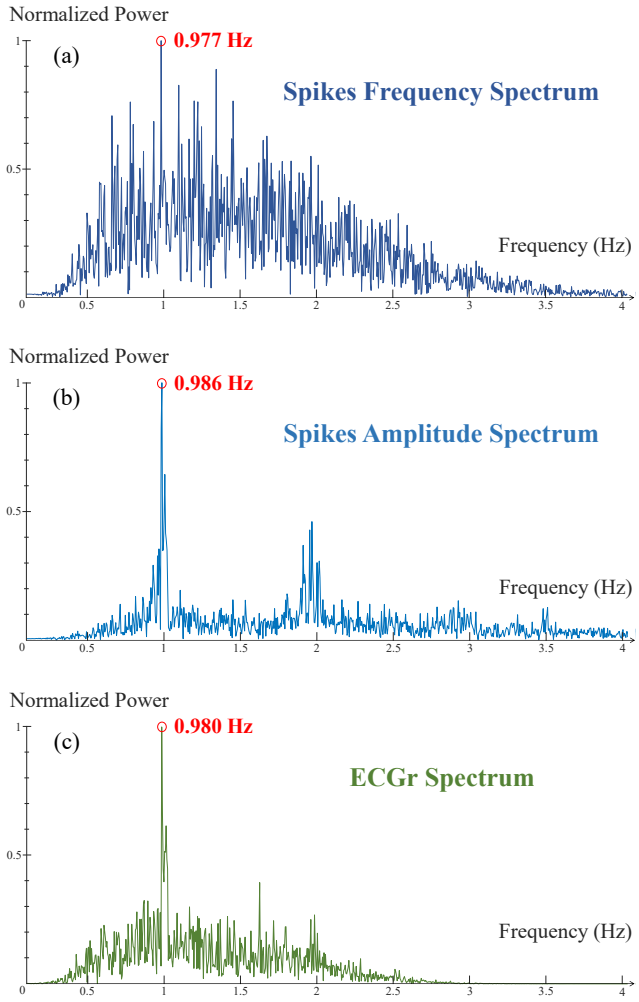

Fig. 5. Frequential spectrums of: (a) the frequency of the detected spikes; (b) the amplitude of the detected spikes; (c) the ECGr. A common peak in the FFT around 0.98 Hz is highlighted.

b). The three modulations are close to each other's, supporting the genuine detection of the APs.

IV. Discussion

We provided an algorithm with simple and efficient methods to detect and cluster the APs, based on [14].

The algorithm could be adapted to other types of nervous activity by changing the template of the first detection. The parameters that can be modified are the template, the correlation thresholds and the maximum discorrelation within a cluster.

One of the limitations is that the algorithm works only offline, limiting its use to signal post-processing. Further work could adapt the algorithm to online processing. One way to do so would be to choose the specific templates during a learning phase (still offline). These specific templates would be stored, and only the second detection would be performed online. This would keep the same procedure and yet drastically reduce the required computing power.

To improve the detection and the classification of APs, other features and clustering methods could be investigated. Clustering using the fuzzy C-mean with principal component analysis, or the superparamagnetic clustering with wavelet decomposition coefficients, are developed in [21] and [22] respectively and could be adapted here.

The validation was made on acute data, detected APs showing amplitude and frequency patterns similar to the ECGr. More robust trials will follow on more specimens and chronic activity, with other physiological markers like the circadian rhythm [23].

V. Conclusion

We proposed an action potential detection algorithm with a versatile template matching and validated it with an acute VENG analysis. It was developed as part of the investigations performed by our group in neural data processing [4], [14], [17], [18], [23], [24]. The algorithm is fully automated, and default parameters are proposed.

We will use the proposed AP detection algorithm to analyze nerve activity in an epileptic framework, in line with our previous works. Besides, our group is also investigating the use of gastric electrical stimulation (GES) as a minimally invasive treatment for obesity [25]–[28]. In that frame, automated AP detection to quantify vagus nerve activity modulation may be used as an indicator to assess the effects of GES and hence optimize the treatment.

More generally, this AP detection algorithm could prove useful in many other applications in neurology where neve activity should be quantified. Adapting to each specific study only requires modifying the generic correlation templates and possibly adapting the three major parameters.

References

[1] I. Pachnis, "Neutralisation of myoelectric interference from recorded nerve signals using models of the electrode impedance," PQDT - UK Irel., no. September, p. 1, 2010, [Online]. Available: https://discovery.ucl.ac.uk/id/eprint/708399

[2] A. Demosthenous, I. Pachnis, D. Jiang, and N. Donaldson, "An integrated amplifier with passive neutralization of myoelectric interference from neural recording tripoles," IEEE Sens. J., vol. 13, no. 9, pp. 3236–3248, 2013, doi: 10.1109/JSEN.2013.2271477.

[3] L. Stumpp et al., "Recording of spontaneous vagus nerve activity during Pentylenetetrazol-induced seizures in rats," J. Neurosci. Methods, vol. 343, Sep. 2020, doi: 10.1016/j.jneumeth.2020.108832.

[4] H. Smets et al., "Analysing vagus nerve spontaneous activity using finite element modelling," J. Neural Eng., vol. 18, no. 5, Oct. 2021, doi: 10.1088/1741-2552/abe68f.

[5] R. R. Harrison, "A Low-Power Integrated Circuit for Adaptive Detection of Action Potentials in Noisy Signals," Annu. Int. Conf. IEEE Eng. Med. Biol. - Proc., vol. 4, pp. 3325–3328, 2003, doi: 10.1109/iembs.2003.1280856.

[6] Dinghan Hu, Jiuwen Cao, Xiaoping Lai, and Junbiao Liu, "Epileptic State Classification based on IntrinsicMode Function and Wavelet Packet Decomposition," 41st Annu. Int. Conf. IEEE Eng. Med. Biol. Soc., pp. 2382–2385, 2019, doi: 10.1109/embc.2019.8856282.

[7] S. Farashi, M. Abolhassani, and M. Taghavi Kani, “An Empirical Mode Decomposition Based Method for Action Potential Detection in Neural Raw Data,” Int. J. Med. Heal. Sci., vol. 8, no. 1, pp. 45–49, 2014.

[8] S. Kim, J. McNames, and K. Burchiel, “Action potential detection with automatic template matching,” Annu. Int. Conf. IEEE Eng. Med. Biol. - Proc., vol. 26 I, pp. 41–44, 2004, doi: 10.1109/iembs.2004.1403085.

[9] S. Kim and J. McNames, “Automatic spike detection based on adaptive template matching for extracellular neural recordings,” J. Neurosci. Methods, vol. 165, no. 2, pp. 165–174, Sep. 2007, doi: 10.1016/j.jneumeth.2007.05.033.

[10] S. Potentials, Y. Hu, H. Liu, and K. D. K. Luk, “Signal-to-Noise Ratio of Intraoperative Tibial Nerve,” vol. 27, no. 1, pp. 3–6, 2010.

[11] S. Raspopovic, J. Carpaneto, E. Udina, X. Navarro, and S. Micera, “On the identification of sensory information from mixed nerves by using single-channel cuff electrodes,” J. Neuroeng. Rehabil., vol. 7, no. 1, pp. 1–15, 2010, doi: 10.1186/1743-0003-7-17.

[12] Sajjad Farashi, Mohammadjavad Abolhassani, and Mostafa Taghavi Kani, “An Empirical Mode Decomposition Based Method forAction Potential Detection in Neural Raw Data,” Int. J. Med. Heal. Sci., vol. 8, pp. 45–49, 2014, doi: doi.org/10.5281/zenodo.1090743.

[13] M. S. Lewicki, “A review of methods for spike sorting: The detection and classification of neural action potentials,” Netw. Comput. Neural Syst., vol. 9, no. 4, 1998, doi: 10.1088/0954-898X_9_4_001.

[14] A. Nonclercq et al., “Cluster-based spike detection algorithm adapts to interpatient and intrapatient variation in spike morphology,” J. Neurosci. Methods, vol. 210, no. 2, pp. 259–265, Sep. 2012, doi: 10.1016/j.jneumeth.2012.07.015.

[15] J. A. Waxenbaum and M. Varacallo, “Anatomy , Autonomic Nervous System. [Updated 2019 Mar 9],” in StatPearls [Internet]. Treasure Island (FL): StatPearls Publishing; 2019 Jan-., 2019.

[16] J. Chávez et al., “Micro cuff electrode manufacture for vagus nerve monitoring in rats,” in IEEE, 2022, pp. 2–6.

[17] L. Stumpp et al., “Recording of spontaneous vagus nerve activity during Pentylenetetrazol-induced seizures in rats,” J. Neurosci. Methods, vol. 343, p. 108832, Sep. 2020, doi: 10.1016/j.jneumeth.2020.108832.

[18] L. Stumpp et al., “Vagus nerve electroneurogram based detection ofacute pentylenetetrazol induced seizures in rats,” Int. J. Neural Syst., 2021.

[19] R. Pallas-Areny, J. Colominas-Balague, and F. J. Rosell, “Effect of respiration-induced heart movements on the ECG,” IEEE Trans. Biomed. Eng., vol. v, no. n, pp. 585–590, 1992.

[20] G. Hahn, I. Sipinkova, F. Baisch, and G. Hellige, “Changes in the thoracic impedance distribution under different ventilatory conditions,” Physiol. Meas., vol. 16, no. 3A, 1995, doi: 10.1088/0967-3334/16/3A/016.

[21] A. Oliynyk, C. Bonifazzi, F. Montani, and L. Fadiga, “Automatic online spike sorting with singular value decomposition and fuzzy C-mean clustering,” BMC Neurosci., vol. 13, no. 1, 2012, doi: 10.1186/1471-2202-13-96.

[22] R. Quian Quiroga and Z. Nadasdy, “Unsupervised Spike Detection and Sorting with Wavelets and Superparamagnetic Clustering,” Neural Comput., vol. 16, pp. 1661–1687, 2004.

[23] H. Smets et al., “Chronic recording of the vagus nerve to analyze modulations by the dark-light cycle,” J. Neural Eng, 2022.

[24] J. Cury et al., “Infrared neurostimulation in ex-vivo rat sciatic nerve using 1470 nm wavelength,” J. Neural Eng., vol. 18, no. 5, 2021, doi: 10.1088/1741-2552/abf28f.

[25] A. Debelle, J. Devière, F. Giannotta, F. Huberland, L. Lonys, and A. Nonclercq, “Tissue Anchoring Assembly,” EP 18213753.9, 2018

[26] L. Lonys et al., “In Vivo Validation of a Less Invasive Gastrostimulator,” Artif. Organs, vol. 41, no. 11, 2017, doi: 10.1111/aor.13056.

[27] A. Debelle et al., “Impact of adaptive gastric electrical stimulation on weight, food intake, and food intake rate in dogs,” Artif. Organs, no. September, pp. 1–13, 2021, doi: 10.1111/aor.14156.

[28] A. Debelle et al., “Optimization and assessment of a novel gastric electrode anchoring system designed to be implanted by minimally invasive surgery,” Med. Eng. Phys., vol. 92, pp. 93–101, 2021, doi: 10.1016/j.medengphy.2021.05.004.